Modulated STM images of ultrathin $MoSe_2$ films grown on $MoS_2(0001)$ studied by STM/STS

H. Murata and A. Koma
Department of Chemistry, Graduate School of Science, The University of Tokyo, Bunkyo-ku, Tokyo 113-0033, Japan
(Received 10 November 1998)

The $MoSe_2/MoS_2$ system is investigated by scanning tunneling microscope (STM) and by its spectroscopic mode, scanning tunneling spectroscopy (STS). STM images show a hexagonal wagon-wheel-like pattern, which is made of bright lines and dark triangles. High-resolution STM images show that the bright line consists of twin lines separated by about 1 nm and that the hexagonal pattern is often skewed. These features are not explained by the simple moiré effect due to the lattice mismatch between the overlayer and the substrate materials. The STS spectra show that the bright area results mainly from electron waves derived from chalcogen orbitals running parallel to the interface between $MoSe_2$ and MoS_2 layers. A mechanism of the pattern formation is proposed, in which scattered electron waves produce the bright wagon-wheel-like pattern.
[S0163-1829(99)02916-1]

I. INTRODUCTION

So far, modulated structures have been observed in scanning tunneling microscope (STM) images of heteroepitaxial ultrathin films of $MoSe_2/SnS_2$,[1] $MoSe_2/MoS_2$,[2,3] Ge(111)/Ga,[4] graphite/Pt,[5] and others.[6,7] Most of them show a long-wavelength structure (superstructure) due to the lattice mismatch between the overlayer and the substrate materials. One of the explanations for the observed superstructure is the vertical atomic displacement of the overlayer of which the lattice is modulated by the underlying lattice-mismatched substrate.[8] That is, the difference of stacking between two layers leads to a height variation in the overlayer, which gives the superstructure in the STM image. That interpretation, however, seems to be improper, since the superstructure is observed even in heterostructures of layered materials.[1–3] This is because vertical displacement would not be so large as the one estimated from topographic STM images in the case of layered materials, in which the interaction between unit layers is such a very weak one as van der Waals interaction. In addition, the superstructure has not been observed in atomic force microscope (AFM) images. Therefore, the vertical atomic displacement is not considered to be the main factor producing the superstructure in those materials, and their superstructure should be interpreted by other mechanism.

Another explanation for the superstructure observed in STM images is moiré interference caused by two lattice-mismatched layers,[5,8] which is often observed in the transmission electron microscope images. The simple moiré interference, however, cannot be applied to STM, since the STM is sensitive to the outermost layer and the signal from the underlying layer should be attenuated during tunneling in the uppermost layer. Furthermore, the detailed structures are different from images calculated by the simple moiré interference even if lateral atomic displacements in the overlayer[9] are taken into account. Therefore, the modulated structure does not seem to come from the simple moiré effect, either.

Recently, other mechanisms have been proposed on the basis of a theoretical study to explain the observed superstructures.[10] Nanoscale structures in the subsurface region are considered to be observable in STM, because waves having nanometer length can propagate through many layers without decay. In this case the contrast of the observed superstructure depends on the overlayer thickness. To our knowledge, such theoretically proposed behavior of STM images has not been observed experimentally so far, and calculated images are different from the observed ones.

Usually atomic displacement appears in the interface of the lattice-mismatched system, and so we cannot identify whether the superstructure observed in an STM image is mainly derived from the vertical atomic displacement or from the interface electronic interaction. In the case of the layered material heterostructures, on the other hand, possibility of the atomic displacement, which causes the strong electronic effect can be excluded, since there is no chemical bond formation at the interface of heterostructures. Thus, we have investigated a system consisting of one monolayer $MoSe_2$ film grown on a cleavage face of MoS_2 by STM in order to clarify the formation mechanism of the modulated structure observed in STM images.

We also have made scanning tunneling spectroscopy (STS) measurement of the modulated structure to investigate the electronic effect, since it gives information on the spatially resolved electronic structures. This feature is lacking in the commonly used spectroscopic methods, such as ultraviolet photoemission spectroscopy (UPS), inverse photoemission spectroscopy (IPES), and electron-energy-loss spectroscopy (EELS).

II. EXPERIMENT

Ultrathin $MoSe_2$ films were grown on the basal plane of a MoS_2 crystal with molecular beam epitaxy.[1] Substrates were cleaved in air and cleaned by heating at 500 °C under ultrahigh vacuum. The mean thickness of the grown film was less than one monolayer. A Knudsen cell and an electron beam evaporator were used as selenium and molybdenum beam sources, respectively. The growth temperature was 450 °C and growth rate was about 0.1 ML/min. The grown specimens were transferred from a growth chamber to an STM chamber of which pressure is 3×10^{-8} Pa. The STM apparatus used in the present investigation was an Omicron VT-

STM unit. STM images and STS spectra were measured at room temperature.

STM images and STS spectra of $MoS_2(0001)$ and $MoSe_2(0001)$ were observed for reference. Single crystals of MoS_2 were natural molybdenite, and single crystals of $MoSe_2$ were grown by the vapor transport method. Before STM and STS measurements they were cleaned by heating at 500 °C under ultrahigh vacuum. STM images were acquired in the constant current mode and were shown as the gray-scale representation, in which brightness increases with decreasing distance between the tip and the sample surface. The sign of the sample bias voltage V_s, which is referred to the Fermi level (E_F), corresponds to the voltage applied to the sample with respect to the tip.

It is difficult to observe the STM image for the ultrathin films of the layered materials, because of the possibility of movement or drift of island of the thin film. Moreover, even if the observed specimen is a pristine transition-metal dichalcogenide, it is not easy to obtain good STS spectra because of local cleavage induced by the tip.[11] It is considered to come from the weak van der Waals interaction between layers. In the case of the heterostructure specimens, it was also hard to obtain good STS spectra with high-spatial resolution and with high-energy resolution because of the above-mentioned difficulties. In order to overcome these difficulties, every spectrum of the heterostructure was obtained by averaging over 100 spectra of equivalent points with the current imaging tunneling spectroscopy (CITS) method.[12] The STS spectra of the bulk specimens shown in the next section are also area-averaged ones. Although spatial information in the atomic scale was lost by the above-mentioned averaging process, some were compensated by atomic-scale STM images taken at various bias voltages.

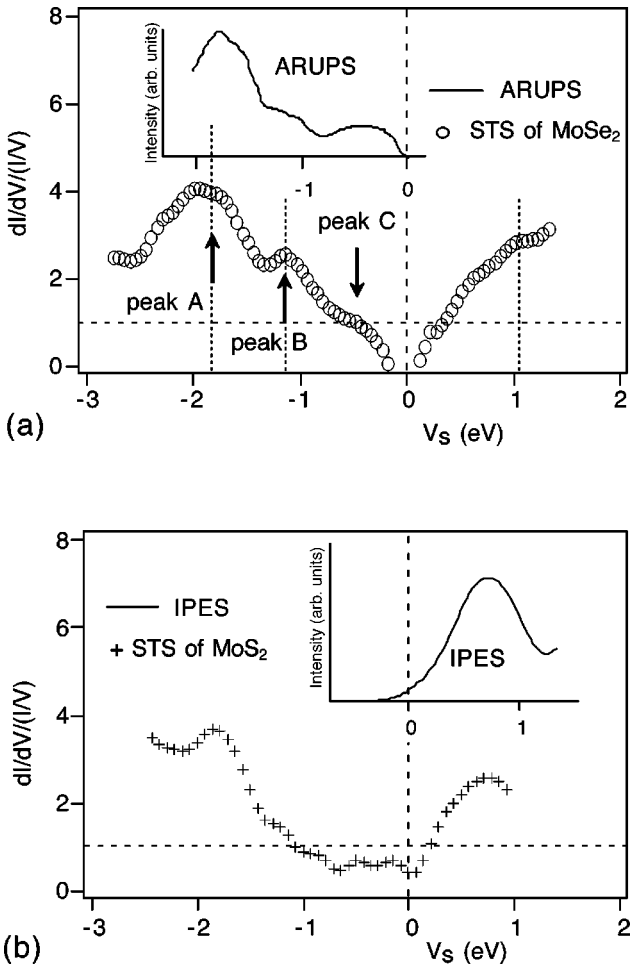

FIG. 1. (a) Normalized differential conductance vs sample bias voltage relative to the Fermi energy of $MoSe_2$ (open circles). Upper curve shows a UPS spectrum (solid line) (Ref. 14). (b) Normalized differential conductance of MoS_2 (cross) and an IPES spectrum (solid line) (Ref. 13). $(dI/dV)/(I/V)$ spectra are calculated from the average of 500 spectra taken for the equivalent areas.

III. RESULTS

A. STM and STS studies of MoS_2 and $MoSe_2$

The STS spectra of MoS_2 and $MoSe_2$, that are spatially averaged, are shown in Fig. 1 in the normalized differential conductance $(dI/dV)/(I/V)$ calculated from I-V data. They are compared with spectra which are obtained by commonly used spectroscopic methods. The conduction band of MoS_2 and the valence band of $MoSe_2$ were investigated by IPES (Ref. 13) and by UPS,[14,15] respectively. The spectrum of $MoSe_2$ in the negative-bias region, which will reflect the occupied states of specimens, is very similar to the density of states (DOS) obtained from UPS, whereas that of MoS_2 in the positive-bias region, which will reflect the unoccupied states, is almost the same as the IPES data. Thus, the present results suggest that STS spectra of two layered materials MoS_2 and $MoSe_2$ reflect their DOS, as was pointed out in Ref. 16 that $(dI/dV)/(I/V)$ reflects the electronic DOS of the specimen.

The global features of the STS spectra of MoS_2 and $MoSe_2$ resemble each other. The resemblance reflects the similarity of the electronic structures of MoS_2 and $MoSe_2$, especially in Mo components. This is because they have chalcogen-substituted structures. However, difference between the two spectra appears in the features in the vicinity of E_F over the range from -1.5 to 0 eV, in which the intensity of the $MoSe_2$ spectrum is larger than that of the MoS_2 spectrum. This difference is considered to be mainly derived from chalcogen-related orbitals (p_x, p_y, p_z orbitals). This conclusion is supported by the bias dependence of the STM images shown in the followings.

The bias dependence of the STM images for MoS_2 was observed, as shown in Fig. 2. In the positive bias region above $+0.5$ V and the negative bias region below -1.5 V, clear STM images were hardly observed, because of a highly noisy signal in the tunneling current. Thus, the bias dependence is presented only in the vicinity of E_F from -1.5 to $+0.5$ V. Figure 2 shows typical STM images for three negative-bias voltages, in which the honeycomb and the spherical structures are observed. When the magnitude of the negative bias is large the honeycomb structure appears [see Fig. 2(c)], whereas the spherical atomic image appears when the negative bias is close to zero [see Fig. 2(a)].

In discussing bias dependence of STM images we must take into account the following points. The tunneling current I is given by the integral over the energy-dependent local density of states (LDOS) multiplied by a barrier factor for tunneling. In a rough approximation, neglecting a weighting factor for the effective tunneling barrier, we assume that

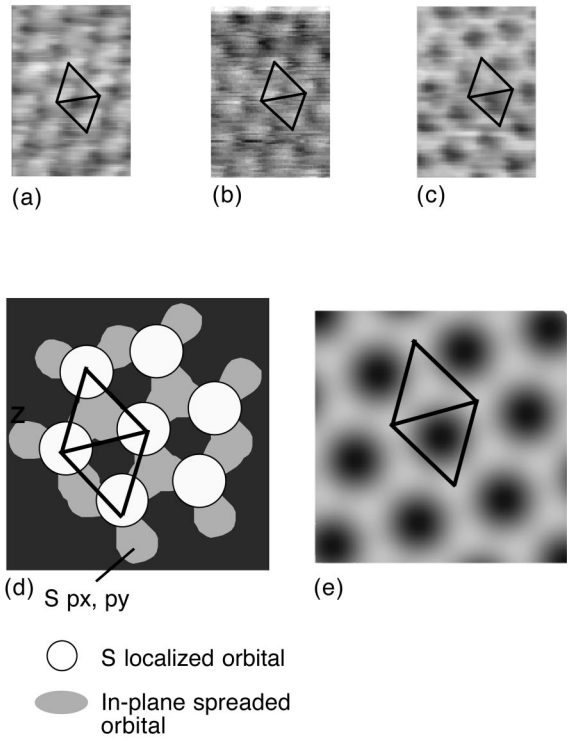

FIG. 2. Topographic images of 1.5×1.0 nm^2 area of $MoS_2(0001)$ at a tunneling current of 0.23 nA. Sample bias voltage (V_s) is (a) -0.31, (b) -1.08, and (c) -1.24 V, respectively. The gray-scale range is (a) 0.16, (b) 0.05, and (c) 0.05 nm, respectively. The images have been corrected for the effect of thermal drift. The (1×1) unit cell is marked in each image. These images are explained by illustrating orbitals shown in (d): empty circle shows S localized p_z orbital, and the gray region corresponds to p_x, p_y orbitals of the outermost layer. (e) shows a gray-scale image of simulated honeycomb pattern [see Eq. (1)].

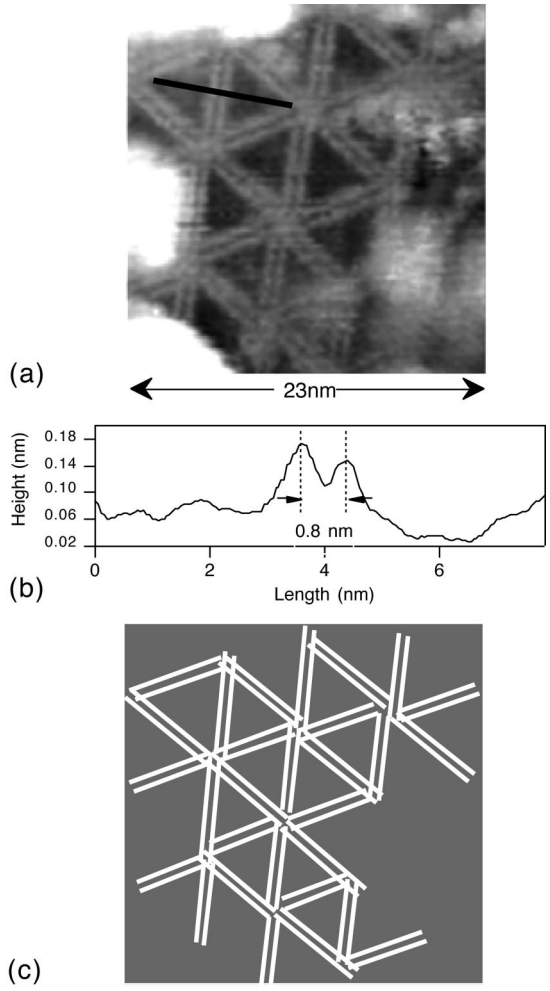

FIG. 3. (a) Typical STM image of the modulated structure for $MoSe_2$ film on MoS_2. Coverage of $MoSe_2$ is less than one monolayer. 23×23 nm^2, $I=0.20$ nA, $V_s=-0.78$ V, constant current mode. (b) Profile along the [1010] of the thick solid line shown in (a). The height of the corrugation depends on the measurement conditions. (c) Schematic drawing of the STM image.

electrons from all occupied states of the specimen between $E_F-e|U|$ and E_F, where U is applied voltage, tunnel into the empty-tip state. Although a detailed discussion will be given elsewhere, it is considered that the images of Fig. 2(a) come from localized atomic orbitals of chalcogen. By increasing the value of negative-bias voltage, low-lying occupied states will contribute to the tunneling current, and the honeycomb structure in Fig. 2(c) results from low-lying in-plane spread orbitals of chalcogen. The image of Fig. 2(b) is a mixture of those two components.

Thus, these STM images in Fig. 2 lead us to the conclusion that there are at least two spatially distinct occupied states near the surface. Below E_F chalcogen localized atomic orbitals are main component at $0--0.7$ eV (peak C), while chalcogen in-plane-spread orbitals are main component at ~-1.2 eV (peak B). These orbitals are schematically illustrated in Fig. 2(d), and STS peaks are assigned by considering these states. This interpretation coincides roughly with the theoretical and other experimental results.[14,15,17–21] This bias dependence will be used in the later discussion on the STM images observed in the $MoSe_2$ film on MoS_2.

B. STM images of $MoSe_2/MoS_2$ heterostructures

Figure 3(a) is a typical STM image of the modulated pattern observed in $MoSe_2/MoS_2$ at a sample bias voltage of -0.8 V. The pattern shows the wagon-wheel-like network, which is made of bright twin lines and dark triangles. This pattern is different from patterns simulated in the previous report,[8] which only gives the observed network period of about 8 nm expected from the lattice mismatch of the MoS_2 substrate and the $MoSe_2$ overlayer.[2,3,8] As shown in Fig. 3(b), each bright line consists of two parallel lines separated by about 1 nm, which lie along the direction parallel to {1120} crystal axes of the $MoS_2(0001)$ surface.[2] Those features are impossible to explain by the simple moiré effect. It is also an important point that symmetry of the pattern is not strictly hexagonal [see Fig. 3(c)]. Although it was reported in a previous paper[8] that the bright lines are continued, these lines have been found to be often discontinued in the present study. Some of twin lines shift each other and discontinuity appears at random.

We have found from detailed STM measurements of $MoSe_2/MoS_2$ heterostructures that the modulated pattern shows bias voltage dependence. When the sample bias voltage is changed, the pattern is clearly seen in the bias voltage

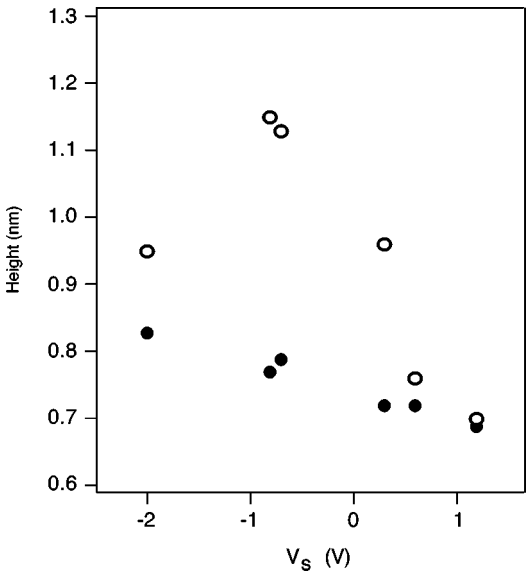

FIG. 4. Bias dependence of the corrugation observed in the STM images of the modulated structure. Curve B (open circle) represents the height of the bright wagon-wheel-like network and curve A (solid circle) shows the height of the dark triangle area. The height is measured from the topmost of the MoS_2 substrate. The used specimen is different from the specimen for Fig. 3.

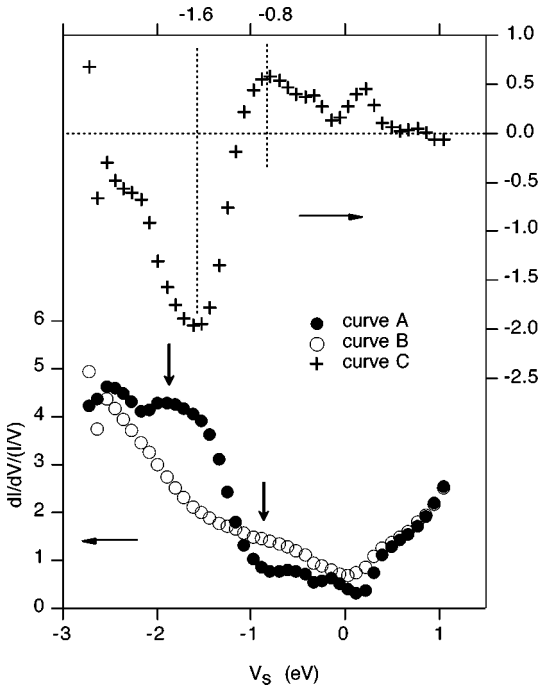

FIG. 5. $(dI/dV)/(I/V)$ spectra of the modulated structure of $MoSe_2/MoS_2$. The curve A (solid circles) show the spectrum of the dark triangle area and the curve B (open circles) show that of the bright wagon-wheel-like network. Every spectrum was obtained from averaging 100 spectra for each area. The curve C (upper panel) shows the difference between curves A and B.

from -2.0 to $+0.3$ V. In this region the height of the dark area measured from the MoS_2 substrate surface is almost constant within 0.7 and 0.8 nm, while the height of the bright area shows a strong bias dependence, as shown in Fig. 4. The height of the dark area is very close to the height of a monolayer of $MoSe_2$, 0.61 nm. This result clearly indicates that the bright twin lines area is enhanced due to electronic modulation, while the dark area shows only a geometric stack. The height difference between the bright and the dark area is much larger than that expected from the possible vertical atomic displacements. Since the magnitude of the observed corrugation for the modulated structure is dependent on measurement conditions, such as the tip apex, feedback loop, and lateral resolution, the amplitude of the corrugation has not been determined precisely, but the overall bias dependence of the ''corrugation height'' can be seen in Fig. 4. As is described in the former section, the pattern has not been observed in AFM images. This result also suggests that the electronic effect produces the modulated STM image.

C. STS analysis of $MoSe_2/MoS_2$ heterostructures

It is usually difficult to connect the STM image directly to the energy-dependent LDOS, because of the complexity of the relation between I and LDOS. Hence, STM topography taken in the constant current mode is inconvenient for understanding electronic structures. In order to understand the bias dependence of the STM images, the spectroscopic method, STS, is the most effective way. Then, we investigated the modulated structure by STS in the CITS mode with bias voltages from -2.5 to $+1.5$ V. In Fig. 5 $(dI/dV)/(I/V)$ vs V_s curves are shown in both the dark (curve A) and the bright (curve B) area. Every spectrum is an average of the value obtained for 100 equivalent points to improve the signal-to-noise ratio. It was found that the width of the band gap in the bright area is smaller than that in the dark area. In the present experiment, the STS spectra did not have so high spatial resolution that we could not individually recognize the bright twin lines. The spectra are compatible with the above-mentioned bias dependence of STM images of the sample.

The two spectra in the bright and the dark area show a large difference in the negative-bias region, while they have almost the same feature for the positive bias. In the bright area of the $MoSe_2$ film, the broad peak is shown around -0.8 eV, but no obvious peak appears around -1.8 eV. In the dark area, on the other hand, the -0.8 eV peak does not appear and a remarkable peak appears at -1.8 eV. The spectrum of the dark area is similar to that of the MoS_2 basal plane in the vicinity of E_F, except for the small peak shift (0.2 eV). This suggests that the dark-triangle area of the $MoSe_2$ film acts as only the tunneling barrier, which may come from the similarity of the electronic structures of MoS_2 and $MoSe_2$ and the long screening length of electrons in semiconducting $MoSe_2$. On the other hand, the spectrum of the bright-line area is clearly different from that of MoS_2. It indicates that the bright area is caused by the electronic modulation with the triangular network structure. Therefore, in order to elucidate the origin of the modulated structure, it is important to discuss the character of the bright area of the $MoSe_2$ film.

In order to clarify the difference in the characters in the dark and bright areas, subtraction of curve (a) from curve (b) has been made and shown as curve (c) in Fig. 5. It is seen that a peak appears at -0.8 eV and a dip at -1.6 eV. With taking into account the peak shift of the spectra for the

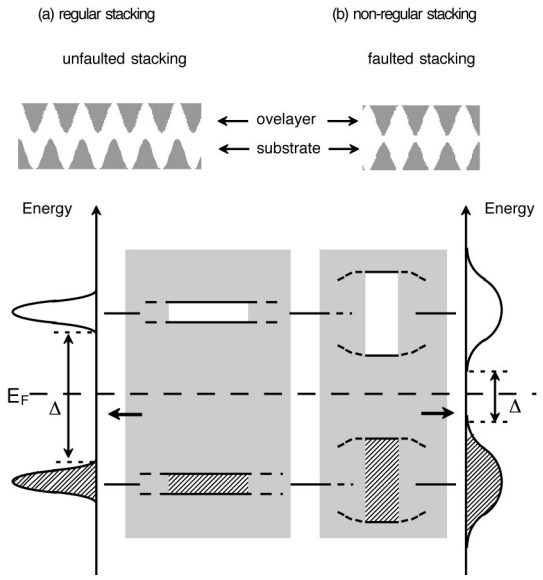

FIG. 6. Schematic view of the formation of states and the band gap for the different stacking at the interface; (a) In-phase stacking (unfaulted stacking), (b) Out-of-phase stacking (faulted stacking). Electronic interaction in the faulted stacking interface is stronger than that of the unfaulted stacking interface, since overlap of interface orbitals in the faulted stacking is larger than that in the unfaulted stacking. The energy width of bands are broadened with increasing electronic interaction, and the density of states (DOS) peak features of the faulted stacking area is broadened compared with that of the unfaulted stacking area. Thus, the width of the band gap Δ in the faulted stacking area is expected to decrease compared with that in the unfaulted stacking area.

modulated pattern with respect to the MoS_2 basal plane, the position of the obtained peak corresponds to -1.0 eV in the spectrum of the basal plane specimens (Fig. 1). The obtained peak is located close to the energy position of peak B of $MoSe_2$ (-1.2 eV), which comes from in-plane spread chalcogen orbitals as was discussed in the previous section. Thus, we suppose in-plane spread chalcogen orbitals play an important role to form the bright area, as will be discussed in the next section.

IV. DISCUSSION

A. Qualitative explanation of the STS spectra

The prominent features of the modulated structure, that is, bright twin lines and the large corrugation lacking in the AFM image, are reproduced neither by the simple moiré interference nor by the atomic displacement. Only the global periodicity of the structure can be explained by the simple moiré effect. The strong bias dependence of the STM images and the STS spectra imply that the modulated structure is due to the electronic effect.

As was pointed out in the previous section, the bright area has narrower band gap and showed broad peak near E_F. On the other hand, the spectrum in the dark area is very similar to that of MoS_2. These features are qualitatively explained by a simple one-dimensional model, as is shown in Fig. 6. Two extreme cases are considered in interface stacking; one is in-phase stacking, and the other is out-of-phase stacking. The latter case of the stacking is often called stacking fault. The electronic interaction between two layers seems to be larger in this case since overlap of interface orbitals in the faulted stacking is larger than that in the unfaulted stacking. The energy width of bands are broadened with increasing electronic interaction, and the density of states (DOS) peak features of the faulted stacking area is broadened compared with that of the unfaulted stacking area as seen in the energy diagram in Fig. 6. Thus, the width of the band gap Δ in the faulted stacking area is expected to decrease compared with that in the unfaulted stacking area. This diagram suggests the narrower band gap and appearance of broad peaks near E_F at the faulted stack region. This model explains the characteristic STS feature of bright areas qualitatively. Thus, if the present model is applied to the heterostructure in the present study, the bright area and the dark area of the modulated structure are considered to correspond to the faulted area and the unfaulted area, respectively. The modulation of valence-band electron states near E_F is shown in the previous band calculation on ultrathin $MoSe_2$ film on MoS_2.[19] It was shown that valence-band electron states near E_F of the $MoSe_2$ overlayer are modulated by the existence of the lattice-mismatched substrate, since wave functions near E_F extend three dimensionally propagating along the c axis through the sandwiches of the layered materials.

The one-dimensional model can explain the present STS results, but it does not explain the observed features of STM images. The model is extended to two-dimensional interface stacking in the next section.

B. Model for explaining the STM images

The way of stacking in the interface was noticed in a previous paper.[8] Effect of the interface was introduced by a simple moiré model, in which two wave functions of substrate and overlayer materials are added. The moiré pattern, however, does not represent the interface interaction strength properly. For example, if one of the wave functions is zero, at some point the interaction should be zero, but the sum of the two wave functions is not always zero. Similarly, the sum of LDOS $(\rho_a+\rho_b)d\tau$ is not an appropriate index for the interface interaction, where ρ_a and ρ_b are LDOS of the substrate and the overlayer materials in the interface, respectively.

In discussing the interface interaction between the substrate and the overlayer, the overlapping position of their wave functions should be considered. In other words, when another layer is stacked on the substrate surface layer, the magnitude of interaction should be represented by the product of LDOS of the two layers. This is mainly because interface interaction between the substrate and overlayer materials is determined by the electron existence probabilities in each layer. Therefore, we will take $\rho_a \cdot \rho_b d\tau$ instead of $(\rho_a + \rho_b)d\tau$.

We assume that ρ_a and ρ_b are composed from wave functions of the Se and S in-plane orbitals since STS results show that contribution of these orbitals seems to be large. The chalcogen in-plane orbitals of the p_x, p_y-like states are modified to the triangle shape by the existence of Mo atoms located in the subsurface [Fig. 2(d)] and the chalcogen in-plane orbitals forms the smeared honeycomb pattern [Fig. 2(e)], which represents the STM images of MoS_2 [Fig. 2(c)]. The

simulated honeycomb pattern, which is shown in Fig. 2(e) was represented by using the expression

$$F(\mathbf{r},\mathbf{g}_1,\mathbf{g}_2)=1+A\left\{\cos[\mathbf{g}_1\cdot\mathbf{r}]+\cos[\mathbf{g}_2\cdot\mathbf{r}]+\cos[(\mathbf{g}_1+\mathbf{g}_2)\cdot\mathbf{r}]+\frac{3}{2}\right\}, \quad (1)$$

where $\mathbf{g_1}$ and $\mathbf{g_2}$ are primitive reciprocal-lattice vectors of substrate surface. Here $F(\mathbf{r},\mathbf{g_1},\mathbf{g_2})$ represents LDOS of in-plane orbitals and the parameter A is chosen as $-2/9$ so that $F(\mathbf{r},\mathbf{g_1},\mathbf{g_2})$ does not become negative. In order to simulate the STM image of interface interaction of layered material heterostructure, the product of $F(\mathbf{r},\mathbf{g_1},\mathbf{g_2})$ and $F(\mathbf{r},\mathbf{g_1'},\mathbf{g_2'})$ was calculated, where $\mathbf{g_1'}$ and $\mathbf{g_2'}$ are primitive reciprocal-lattice vectors of overlayer surface. Here $F(\mathbf{r},\mathbf{g_1},\mathbf{g_2})$ and $F(\mathbf{r},\mathbf{g_1'},\mathbf{g_2'})$ represent the LDOS of the substrate and overlayer in the heterostructure interface, respectively. Magnitude of $\mathbf{g_i'}$ was chosen by 10% larger than $\mathbf{g_i}$, and direction of $\mathbf{g_i'}$ was aligned with $\mathbf{g_i}$, respectively. This pattern well reproduces the triangular superstructure divided by straight lines, as shown in the schematic image of Fig. 7(b). The way of stacking in the gray area (area A) and the white area (area B) illustrated are in-phase stacking and out-of-phase stacking, respectively. Thus, we call the areas A and B as unfaulted and faulted stacking area, respectively.

On the other hand, if p_z-like chalcogen orbitals are taken, which are localized on the atomic position, then we obtain the simulated image of Fig. 7(c). This pattern cannot reproduce the observed STM images, in particular the trigonal structural features. This indicates that in-plane spread p_x, p_y orbitals are responsible for the STM image.

C. Twin-line structure

The simulated pattern of Fig. 7(b), which was discussed in the previous section, is still incomplete since the network of twin lines is not reproduced. We propose a new mechanism for the pattern formation of the modulated structure that scattered electron waves produce the bright wagon-wheel-like structure. This mechanism is similar to brightness enhancement due to the standing wave formation observed at steps on the Au(111) surface in a $(dI/dV)/(I/V)$ image.[22] In case of $MoS_2/MoSe_2$, heterostructure unfaulted stacking (area A) and faulted stacking area (area B) are formed, as was mentioned in the previous section. Difference of interface stacking produces potential variation in the overlayer. The faulted area seems to act as a potential barrier for in-plane electron waves in the overlayer, since the area is energetically unfavorable. The faulted area is located between the two unfaulted areas and the boundary line between the faulted and unfaulted areas is parallel to the lattice vector of the overlayer and substrate. In-plane electron waves traveling to the right and left directions are scattered at both sides of the faulted area. Thus, scattered electrons produce a twin-line structure parallel to the lattice vector. The main component of the scattering electrons is considered to be derived from electron waves that are traveling in the faulted area rather than those in the unfaulted area, as is observed in electron wave scattering near the Au(111) steps.[22]

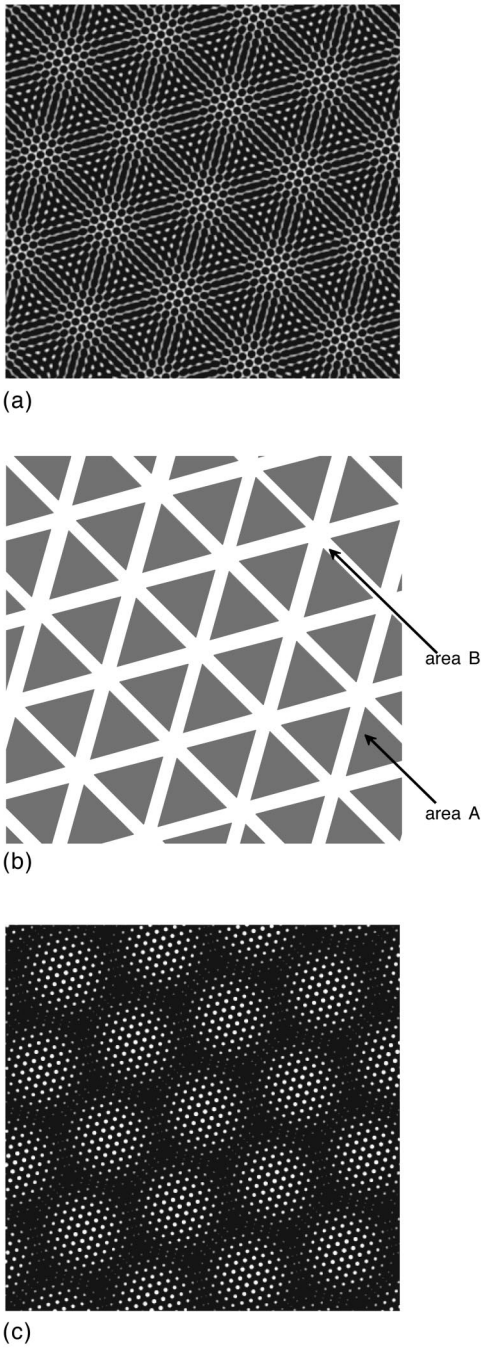

FIG. 7. Superposition of two sets of lattices with periods different by 10%. (a) Product of two mismatched honeycomb waves. (b) Schematic image of (a). Stacking between two lattices is faulted in area B (white) and unfaulted in area A (gray). (c) Product of two mismatched localized atomic waves.

D. Skewed hexagonal structure

Finally, we would like to discuss the origin of the skewed hexagonal structure observed in the wagon-wheel-like network. The slight difference from the hexagonal symmetry of $MoS_2(0001)$ can be explained only by a little modification. The structure is represented by the product of two regular honeycomb waves with a period different by 10% and a stacking of the overlayer rotated by only 1.0°. The simulated pattern is shown in Fig. 8(a). Only 1.0° rotation of the overlayer with respect to the substrate gives remarkable change

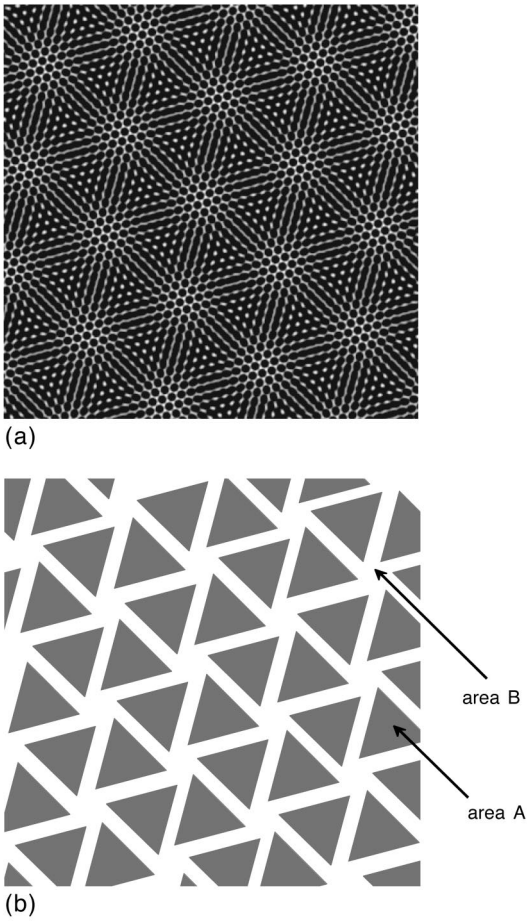

FIG. 8. (a) Product pattern of two honeycomb waves with periods different by 10% and with directions rotated by 1.0°. (b) Schematic image of (a). Skewed structure is clearly formed by the rotation even by using two homogeneous honeycomb waves.

in the triangular network, as is shown in Fig. 8(b). Discontinuities of bright-line areas appear in the figure. The amount of the discontinuity is determined by the rotation angle of the overlayer and the degree of the lattice mismatch.[23] In the case of the $MoSe_2/MoS_2$ heterostructure (the lattice mismatch is 4.1%) only 0.3° rotational angle would produce 1-nm discontinuity of the bright-line areas. Such a small rotation angle is quite unusual, and it is considered to come from other factors that cannot be understood by a mass density wave proposed by McTague and Novaco.[24] It must be noted that the boundary line between two areas in Fig. 8(b) seems to be almost parallel to the lattice vector of overlayer or substrate. This model represents the characteristic properties of the observed STM images. The present model is clearly different from a recent theoretical calculation[25] in which lattice distortion was predicted by the Monte Carlo simulation.[9]

Although we referred the modulated structure as ''moiré structure'' in previous papers, it is concluded that the modulated structure is not caused by the ''moiré'' effect, but by the electronic interaction in the present paper. Therefore, it seems to be more appropriate to call it the modulated structure or the superstructure hereafter.

V. CONCLUSION

The thin $MoSe_2$ film on the MoS_2 system has been investigated in detail by STM and STS. The wagon-wheel-like structure made of the bright twin lines was observed in STM with the skewed hexagonal lattice. The STM images show the strong bias dependence. Although the observed image was previously explained by the simple moiré effect, a new mechanism is proposed to explain the high-resolution STM images observed in the present experiment. STM and STS were observed in MoS_2 and $MoSe_2$ for a reference. It has been found from STS spectra taken for the $MoSe_2/MoS_2$ heterostructure that the bright area mainly results from in-plane spread chalcogen orbitals. The modulated images are enhanced by scattered electron waves at the edge of the unfaulted area. This model also reproduces the superstructure, which has been observed in the similar STM images of the thin $MoSe_2$ film on SnS_2.[1]

ACKNOWLEDGMENTS

The present paper is supported by a Grant-in-Aid for scientific research from the Ministry of Education, Science and Culture.

[1] F. S. Ohuchi, B. A. Parkinson, K. Ueno, and A. Koma, J. Appl. Phys. **68**, 2168 (1990).
[2] F. S. Ohuchi, T. Shimada, B. A. Parkinson, K Ueno, and A. Koma, J. Cryst. Growth **111**, 1033 (1991).
[3] B. A. Parkinson, F. S. Ohuchi, K. Ueno, and A. Koma, Appl. Phys. Lett. **58**, 472 (1991).
[4] M. Böhringer, P. Molinàs-Mata, E. Artacho, and J. Zegenhagen, Phys. Rev. B **51**, 9965 (1995).
[5] T. A. Land, T. Michely, R. J. Behm, J. C. Hemminger, and G. Gomsa, Surf. Sci. **264**, 261 (1992).
[6] H. Itoh, T. Ichinose, C. Oshima, T. Ichinokawa, and T. Aizawa, Surf. Sci. Lett. **254**, L437 (1991).
[7] R. Strohmaier, C. Ludwig, J. Petersen, B. Gompf, and W. Eisenmenger, Surf. Sci. **318**, L1181 (1994).
[8] T. Mori, H. Abe, K. Saiki, and A. Koma, Jpn. J. Appl. Phys. **32**, 2945 (1993).
[9] C. Itoh, T. Miyazaki, K. Aizawa, H. Aoki, and M. Okazaki, J. Phys. C **21**, 4527 (1988).
[10] K. Kobayashi, Phys. Rev. B **53**, 11 091 (1996).
[11] M. G. Youngquist and J. D. Baldeschwieler, J. Vac. Sci. Technol. B **9**, 1083 (1991).
[12] R. J. Hamers, R. M. Tromp, and J. E. Demuth, Phys. Rev. Lett. **56**, 1972 (1986).
[13] M. Sancrotti, l. Braicovich, C. Chemelli, and G. Trezzi, Solid State Commun. **66**, 593 (1988).
[14] R. Coehoorn, C. Haas, J. Dijkstra, C. J. F. Flipse, R. A. de Groot, and A. Wold, Phys. Rev. B **35**, 6195 (1987).
[15] K. Fives, T. McGovern, R. McGrath, R. Cimino, G. Hughes, A. McKinley, and G. Thornton, J. Phys.: Condens. Matter **4**, 5639 (1992).
[16] J. A. Stroscio, R. M. Feenstra, and A. P. Fein, Phys. Rev. Lett. **57**, 2579 (1986).

[17] M. Weimer, J. Kramar, C. Bai, and J. D. Baldeschwieler, Phys. Rev. B **37**, 4292 (1988).
[18] S. Inoue, H. Kawami, M. Yoshimura, and T. Yao, in *Determining Nanoscale Physical Properties of Materials by Microscopy and Spectroscopy*, edited by M. Sarikaya, H. K. Wickramasinghe, and M. Isaacson, MRS Symposia Proceedings No. 332 (Materials Research Society, Pittsburgh, 1994), p. 293.
[19] K. Kobayashi and J. Yamauchi, Phys. Rev. B **51**, 17 085 (1995).
[20] T. Mori, K. Saiki, and A. Koma, Jpn. J. Appl. Phys., Part 2 **31**, L1370 (1992).
[21] R. Coehoorn, C. Haas, and R. A. de Groot, Phys. Rev. B **35**, 6203 (1987).
[22] Y. Hasegawa and Ph. Avouris, Phys. Rev. Lett. **71**, 1071 (1993).
[23] T. Wiederholt, H. Brune, J. Wintterlin, R. J. Behm, and G. Ertl, Surf. Sci. **324**, 91 (1995).
[24] J. P. McTague and A. D. Novaco, Phys. Rev. B **19**, 5299 (1979).
[25] K. Kobayashi, J. Vac. Sci. Technol. B **14**, 1075 (1996).